International Journal of Heat and Mass Transfer 52 (2009) 3147–3158

Contents lists available at ScienceDirect

International Journal of Heat and Mass Transfer

journal homepage: www.elsevier.com/locate/ijhmt

Subcooled flow boiling heat transfer of R-407C and associated bubble characteristics in a narrow annular duct

C.A. Chen, W.R. Chang, K.W. Li, Y.M. Lie, T.F. Lin *

Department of Mechanical Engineering, National Chiao Tung University, Hsinchu, 1001 Ta Hsueh Road, Hsinchu 30010, Taiwan, ROC

ARTICLE INFO

Article history:
Received 29 July 2008
Received in revised form 29 January 2009
Accepted 29 January 2009
Available online 28 March 2009

Keywords:
Subcooled flow boiling
R-407C
Bubble characteristics
Heat transfer
Mini-channel

ABSTRACT

An experiment is conducted here to investigate how the channel size affects the subcooled flow boiling heat transfer and the associated bubble characteristics of refrigerant R-407C in a horizontal narrow annular duct with the gap of the duct fixed at 1.0 and 2.0 mm. The measured boiling curves indicate that the temperature overshoot at ONB is relatively significant for the subcooled flow boiling of R-407C in the duct. Besides, the subcooled flow boiling heat transfer coefficient increases with a reduction in the duct gap, but decreases with an increase in the inlet liquid subcooling. Moreover, raising the heat flux imposed on the duct can cause a significant increase in the boiling heat transfer coefficients. However, the effects of the refrigerant mass flux and saturated temperature on the boiling heat transfer coefficient are slighter. Visualization of the subcooled flow boiling processes in the duct reveals that the bubbles are suppressed to become smaller and less dense by raising the refrigerant mass flux and inlet subcooling. Raising the imposed heat flux, however, produces positive effects on the bubble population, coalescence and departure frequency. Meanwhile, the present heat transfer data for R-407C are compared with the R-134a data measured in the same duct and with some existing correlations. We also propose empirical correlations for the present data for the R-407C subcooled flow boiling heat transfer and some quantitative bubble characteristics such as the mean bubble departure diameter and frequency and the active nucleation site density.

1. Introduction

Choosing a suitable refrigerant plays the most important part in the design of air conditioning and refrigeration systems. In addition, the chlorofluorocarbons refrigerants (CFCs) have been completely prohibited in production since 1996 and the hydrochlorofluorocarbons refrigerants (HCFCs) are planned to be phased out by 2020, due to the presence of chlorine and carbon in these refrigerants which are depleting the earth's stratospheric ozone layer and increasing the Total Equivalent Warming Impact (TEWI). Thus, the substitution of CFCs and HCFCs becomes urgent recently. The hydrofluorocarbons refrigerants (HFCs) such as R-134a, R-407C, R-410a, R-410b and R-507 are considered to be the eligible alternatives and some are currently in use.

In air conditioning and refrigeration systems, small channel with its small volume, lower total mass and low inventory of working fluid is an appropriate option for the compact heat exchangers to improve the boiling and condensation heat transfer performance. It is important to comprehend the boiling and condensation heat transfer and flow characteristics in the small channels consisted in compact heat exchangers. The channels size in a compact heat exchanger can significantly affect the performance of the exchanger [1]. In sizing the small channels, Kandlikar and Grande [2] proposed that for the conventional channels D_h >3 mm, for the mini-channels 200 μm < D_h < 3 mm, and for the micro-channels 10 μm < D_h < 200 μm. On the contrary, Kew and Cornwell [3] introduced the Confinement number, $N_{conf} = \frac{(\sigma/(g\Delta\rho))^{0.5}}{D_h}$, which represents the importance of the flow restriction by the small size channel. They showed that the effects of the channel size became extremely substantial when N_{conf} > 0.5.

Investigation of refrigerants R-11 and R-123 flow boiling in a horizontal small copper tube (D_h = 1.95 mm) by Bao et al. [4] showed that the heat transfer coefficients were independent of the refrigerant mass flux and vapor quality, but were function of the wall heat flux. Nucleate boiling was the dominant mechanism over a wide range of the tested flow conditions. Tran et al. [5] examined refrigerant R-12 flow boiling in small circular and rectangular channels (D_h = 2.46 and 2.4 mm). Two distinct two-phase flow regions were noted, the convective boiling dominant region at lower wall superheat (<2.75 K) and nucleate boiling dominant region at higher wall superheat (>2.75 K). The differences in the boiling heat transfer coefficients in the circular and rectangular tubes are small. The R-134a experimental data taken from an upward vertical rectangular multi-channel (D_h = 2.01 mm) by Agostini and Bontemps [6] concluded that bubble nucleation was the

* Corresponding author.
E-mail address: tflin@mail.nctu.edu.tw (T.F. Lin).

0017-9310/$ - see front matter © 2009 Elsevier Ltd. All rights reserved.
doi:10.1016/j.ijheatmasstransfer.2009.01.027

Nomenclature

A_s	outside surface area of the heated inner pipe, m^2
Bo	Boiling number, $Bo = \frac{q}{G \cdot i_{fg}}$, dimensionless
c_p	specific heat, J/kg°C
D_i, D_o	inner and outside diameters of duct, m
D_h	hydraulic diameter, m, $D_h = (D_o - D_i)$
D_p	dimensionless mean bubble departure diameter
d_P	bubble departure diameter, m
F_d	dimensionless mean bubble departure frequency
f	bubble departure frequency
Fr	Froude number, $Fr = \frac{G^2}{\rho_l^2 \cdot g \cdot D_h}$, dimensionless
f_f	friction factor
g	acceleration due to gravity, m/s^2
G	mass flux, kg/m^2s
h_r	boiling heat transfer coefficient, $W/m^2°C$
i_{fg}	enthalpy of vaporization, J/kg
k_l	liquid thermal conductivity, W/m°C
n_{ac}	active nucleation site density, n/m^2
N_{AC}	dimensionless active nucleation site density
N_{conf}	Confinement number, $N_{conf} = \frac{(\sigma/(g\Delta\rho))^{0.5}}{D_h}$, dimensionless
Ja	Jakob number, $Ja = \frac{\rho_l \cdot C_p \cdot \Delta T_{sub}}{\rho_g \cdot i_{fg}}$, dimensionless
Nu	Nusselt number, $Nu = \frac{hD_h}{k}$, dimensionless
P	system pressure, kpa
Pr	Prandtl number, $\mathrm{Pr} = \mu \cdot c_p/k$, dimensionless
q	average imposed heat flux, W/m^2
q_b, q_c, q_t	heat flux due to bubble nucleation, single-phase convection, total value, W/m^2
Q_n	net power input, W
$\mathrm{Re_l}$	liquid Reynolds number in two-phase flow, $Re_l = \frac{GD_h(1-x)}{\mu_l}$, dimensionless
T_r, $T_{r,i}$	mean, inlet temperature of liquid refrigerant, °C
T_{sat}	saturated temperature of refrigerant, °C
T_w	wall temperature of heated inner pipe, °C
x	vapor quality
z	downstream coordinate for annular duct flow, mm

Greek symbols

ΔT_{sat}	wall superheat, $(T_w - T_{sat})$, °C
ΔT_{sub}	inlet subcooling, $(T_{sat} - T_{r,i})$, °C
δ	gap size, mm
μ_l	viscosity of liquid refrigerant, $N \cdot s/m^2$
ρ_g, ρ	vapor and liquid densities, kg/m^3
$\Delta\rho$	density difference, $\Delta\rho = \rho_l - \rho_g$, kg/m^3
σ	surface tension, N/m

dominant mechanism for the heat flux higher than 14 kW/m^2 and wall superheat higher than 3 K, and the transition from the boiling dominated by bubble nucleation to convection occurred at $Bo \cdot (1 - x) \approx 2.2 \times 10^{-4}$. Kandlikar and Steinke [7] found that for a fluid with a high liquid-to-vapor density ratio, the convective effects dominated as the vapor quality increased. This led to an increasing trend in the boiling heat transfer coefficient at increasing vapor quality. A high boiling number results in a higher nucleate boiling contribution, which tends to decrease as the vapor quality increases, causing a decreasing trend in heat transfer coefficient with increasing vapor quality. An experimental study for the refrigerant R-141b flow boiling in a vertical tube (D_h = 1 mm) conducted by Lin et al. [8] concluded that at low vapor quality nucleate boiling dominated and at higher vapor quality convective boiling dominated. In a review article, Watel [9] concluded that convective boiling dominated at low heat fluxes and wall superheats and high vapor qualities otherwise nucleate boiling dominated.

It has been known for some time that bubble characteristics such as bubble departure frequency, growth, sliding and departure size play an important role in flow boiling heat transfer. Chang et al. [10] examined the behavior of near-wall bubbles in subcooled flow boiling of water in a vertical one-side heated rectangular channel (D_h = 4.44 mm) and described the coalescence of the bubbles. Similar study for subcooled flow boiling of upward water in a vertical annular channel (D_h = 19 mm) conducted by Situ et al. [11] indicated that the bubble departure frequency increased with the heat flux. Outcomes from Yin et al. [12] for R-134a in a horizontal annular duct (D_h = 10.31 mm) showed that the bubble generation was suppressed by raising the refrigerant mass flux and subcooling, and only the liquid subcooling exhibited a significant effect on the bubble size. The study of water boiling in a one side heated horizontal rectangular channel (D_h = 40 mm) conducted by Maurus et al. [13] manifested that the waiting time between two bubble cycles decreased significantly at increasing mass flux. An experimental study on the bubble rise path after its departure from a nucleation site for water in a vertically upward tube (D_h = 20 mm) by Okawa et al. [14] suggested that the inertia force significantly influenced the onset of bubble detachment and the shear force induced a lift force to detach the bubble from the wall. FC-87 flow boiling in a vertical rectangular channel (D_h = 12.7 mm) investigated by Thorncroft et al. [15] manifested that both the bubble growth and departure rates increased with an increase in the Jacob number and the bubble departure diameter decreased with the mass flux. Low pressure subcooled flow boiling inside a vertical concentric annulus (D_h = 13 mm) examined by Zeitoun and Shoukri [16] showed that the mean size and lift duration of the bubbles increased at decreasing liquid subcooling.

Chen [17] proposed an early general empirical correlation model for flow boiling in channels which divided the boiling heat transfer coefficient into two parts: a microconvective (nucleate boiling) contribution estimated by the pool boiling correlations and a macroconvective (non-boiling forced convection) contribution estimated by the single-phase correlation. In order to account for the diminished contribution of nucleate boiling as the forced convective effects increased at a higher vapor quality, he introduced an enhancement factor E and a suppression factor S to respectively accommodate the forced convection augmentation and nucleate boiling retardation. Gungor and Winterton [18] modified the Chen's correlation and proposed the correlations for the enhancement and suppression factors. A general subcooled flow boiling correlation based on a large amount of data measured from pipes and annuli was developed by Shah [19]. An improved correlation from Liu and Winterton [20] introduced an asymptotic function to predict the heat transfer coefficient for vertical and horizontal flows in tubes and annuli. Later, Zhang et al. [21] modified the Chen's correlation to predict the heat transfer in mini channels. Besides, Tran et al. [5] modified the heat transfer correlation of Lazarek and Black [22] with the Reynolds number of the flow replaced by the Weber number to eliminate viscous effects in favor of the influences from the surface tension. Similar correlations were proposed by Fujita et al. [23]. Kandlikar [24] divided the subcooled flow boiling into the partial boiling, fully developed boiling and significant void flow regions. Meanwhile, appropriate correlations were presented to predict the heat transfer in the each region. In a following study [25], he developed correlations to predict transition, laminar and deep laminar flows in mini-channels and micro-channels.

The above literature review clearly indicates that the flow boiling heat transfer of HFC refrigerants in small diameter channels

remains largely unexplored. In a recent study [26], we measured the saturated flow boiling heat transfer and investigated the associated bubble characteristics for R-407C in a horizontal narrow annular duct. In this continuing study, we move further to explore the heat transfer and bubble behavior in subcooled boiling flow of R-407C in the same duct. The effects of the imposed heat flux, gap size, and R-407C mass flux, inlet subcooling and refrigerant saturated temperature on the boiling heat transfer characteristics will be examined in detail. Particularly, flow visualization is conducted to examine the bubble characteristics such as the mean bubble departure diameter and frequency from the heating surface, intending to improve our understanding of the subcooled flow boiling processes in a narrow channel. Data from this study for R-407C will be compared with those for R-134a reported in the previous study [27] and with some existing correlations for small diameter channels proposed in the open literature.

2. Experimental apparatus and procedures

The experimental system employed in the previous study [26] is also used here to investigate the subcooled flow boiling of R-407C in a narrow annular duct. It is schematically depicted in Fig. 1. The experimental apparatus consists of three main loops, namely, a refrigerant loop, a water–glycol loop, and a hot-water loop. As schematically shown in Fig. 2, the test section of the apparatus is a horizontal annular duct with the outer pipe made of Pyrex glass to permit the visualization of boiling processes in the refrigerant flow. The glass pipe is 160 mm long with an inside diameter of 20.0 mm. Its wall is 4.0 mm thick. Both ends of the pipe are connected with copper tubes of the same size by means of flanges and are sealed by O-rings. The inner copper pipe has 16.0 or 18.0-mm nominal outside diameter with its wall being 1.5 or 2.5 mm thick and is 0.41 m long. Thus the gap of the annular duct is 2.0 or 1.0 mm (D_h = 4.0 or 2.0 mm). Note that the outside surface of the inner pipe is polished by fine sandpaper. Besides, to insure the gap between the inner and outer pipes being uniform, we first measure the outside diameter of the inner pipe and the inside diameter of the glass pipe by digital calipers whose resolutions are 0.001 mm with the measurement accuracy of ±0.01 mm. Then we photo the top and side view pictures of the annular duct and measure the average radial distance between the inside surface of the glass pipe to the outside surface of the inner tube. From the above procedures the duct gap is ascertained and its uncertainty is estimated to be 0.02 mm. It is also noted that the flow enters the duct long before the heated section so that the entrance effects on the boiling are small. An electric cartridge heater of 160 mm in length and 13.0 mm in diameter with a maximum power output of 800 W is inserted into the inner pipe. Furthermore, the pipe has an inactive heating zone of 10-mm long at each end and is insulated with Teflon blocks and thermally nonconducting epoxy to minimize heat loss from it. Thermal contact between the heater and the inner pipe is improved by coating a thin layer of heat-sink compound on the heater surface before the installation of the heater. Then, 8 T-type calibrated thermocouples are electrically insulated by electrically nonconducting thermal bond before they are fixed on the inside surface of the inner pipe so that the voltage signals from the thermocouples are not interfered with

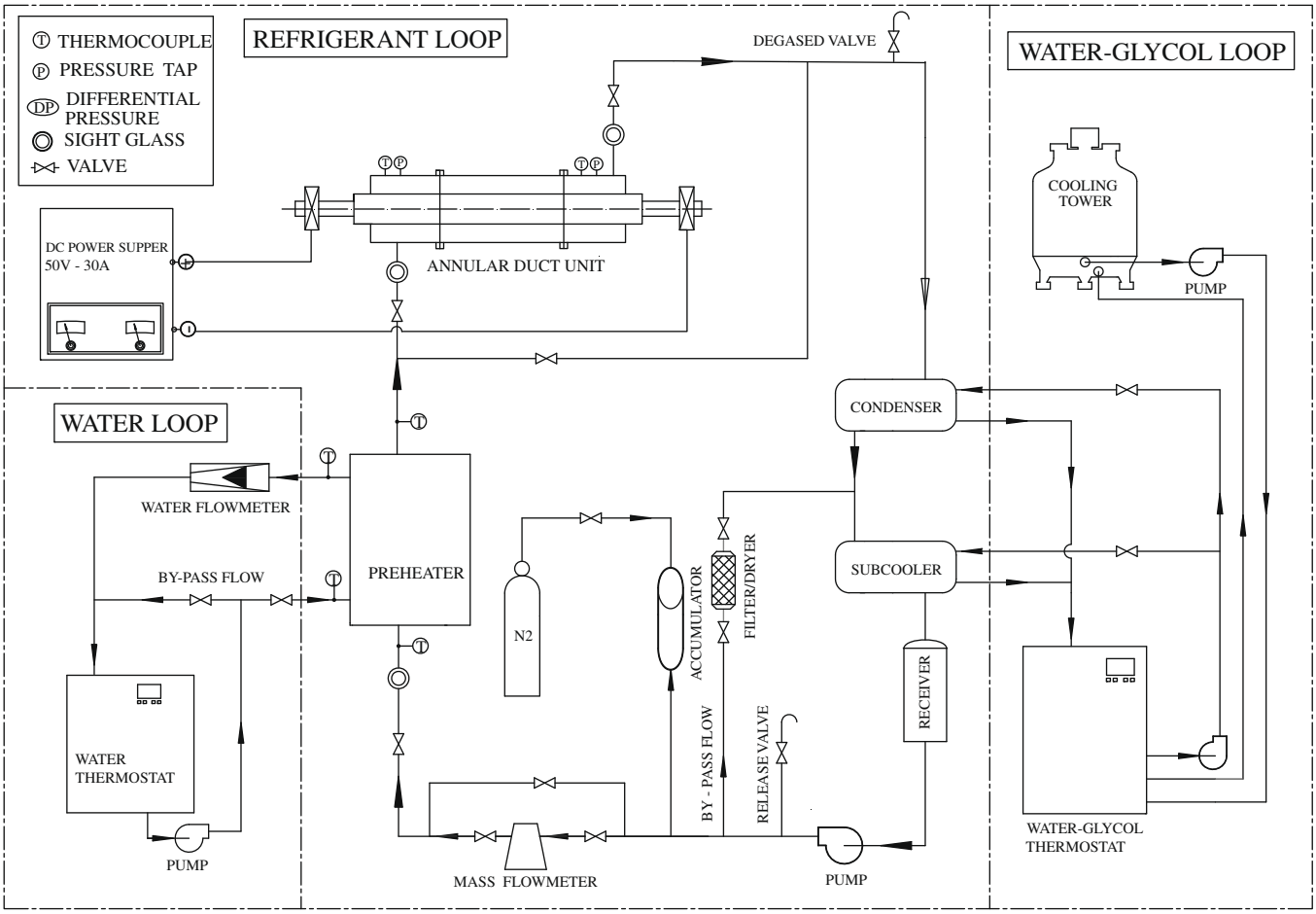

Fig. 1. Schematic of experimental system for the annular duct.

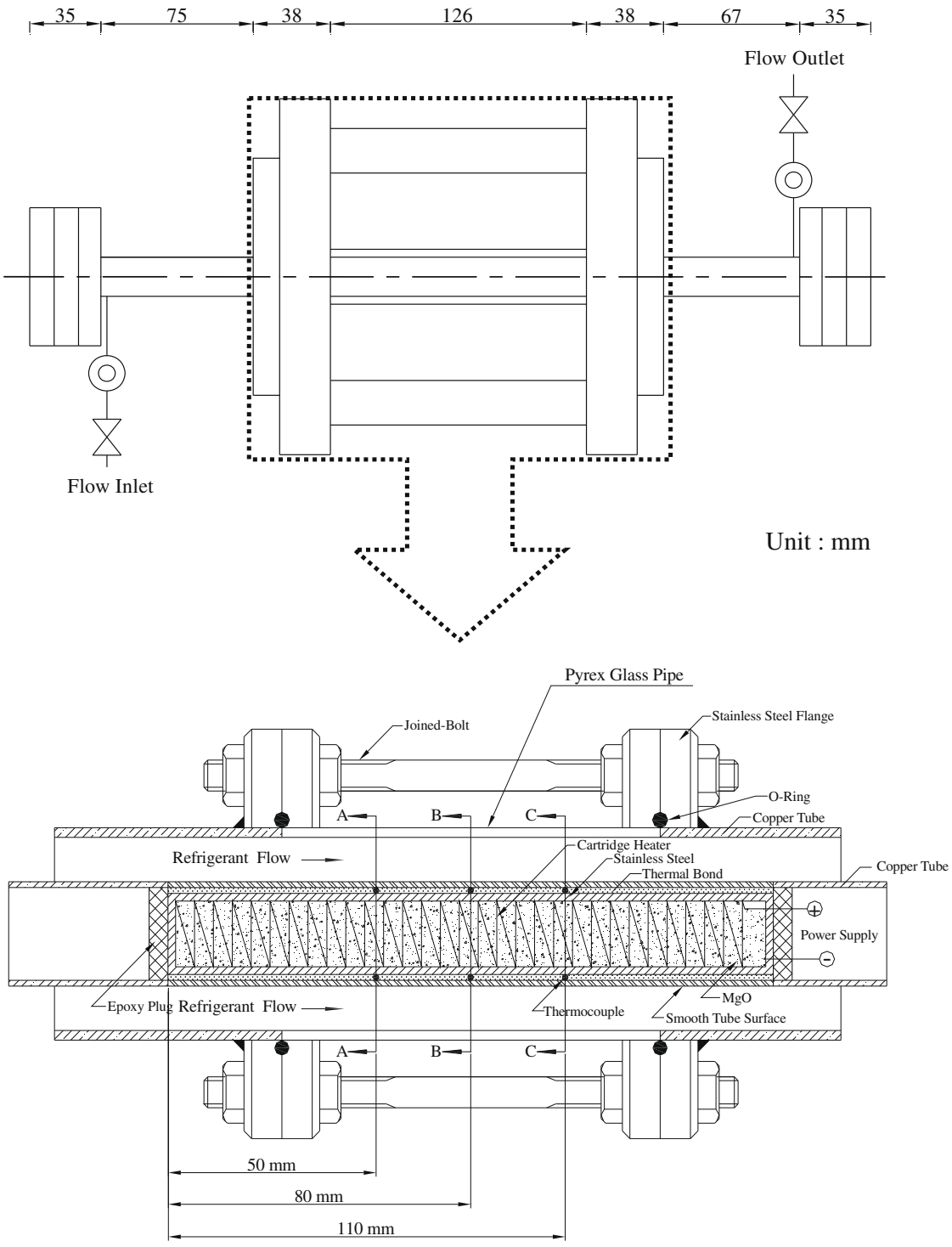

Fig. 2. The detailed arrangement of the test section for the annular duct.

the DC current passing through the cartridge heater. The thermocouples are positioned at three axial stations along the inner pipe. At each axial station, two to four thermocouples are placed at top, bottom, or two sides of the pipe circumference with 180° or 90° apart. The outside surface temperature of the inner pipe T_w is then derived from the measured inside surface temperature by taking into account the radial heat conduction through the pipe wall. The details of the three loops, photographic apparatus, data acquisition unit, and experimental procedures are already available in our early studies [26–28] and are not repeated here. The data repeatability is insured by measuring each data point three times and the deviations of the measured values from their average should be all less than 5%.

3. Data reduction and verification of experimental system

The imposed heat flux q to the refrigerant flow in the annular duct is calculated on the basis of the net power input Q_n and the total outside surface area of the inner pipe of the annular duct A_s

as $q = Q_n/A_s$. The total power input Q_t is obtained from the product of the measured voltage drop across the cartridge heater and electric current passing through it. Hence the net power input to the test section is equal to $(Q_t - Q_{loss})$.

The total heat loss from the test section Q_{loss} is evaluated from the correlation of Churchill and Chu [29] for natural convection around a circular cylinder. To reduce the heat loss from the test section, it is covered with a polyethylene insulation layer. The outcomes from this heat loss test indicate that the total heat loss from the test section is generally less than 1% of the total power input no matter when single-phase or two-phase boiling flow is in the duct. The subcooled flow boiling heat transfer coefficient at a given axial location is defined as

$$h_r = \frac{Q_n/A_s}{(T_w - T_r)} \tag{1}$$

Here T_r is the local bulk liquid refrigerant temperature and at the middle axial location it is approximated by the equation

$$T_r = \frac{T_{r,i} + T_{r,o}}{2} \tag{2}$$

Uncertainties of the measured heat transfer coefficients are estimated according to the procedures proposed by Kline and McClintock [30] for the propagation of errors in physical measurement. The results from this uncertainty analysis are summarized in Table 1.

In order to check the suitability of the experimental system for measuring the subcooled flow boiling heat transfer coefficients, the single-phase liquid R-407C heat transfer data for the liquid Reynolds number ranging from 3459 to 14,640 are measured first and compared with the well-known traditional forced convection correlation proposed by Gnielinski [31], as that in the previous study [26–28]. The results manifest that the present data can be well correlated by their correlation with a mean absolute error of 3.9%. Thus the established system is considered to be suitable for the present subcooled R-407C flow boiling experiment.

4. Results and discussion

The present R-407C subcooled flow boiling experiments are performed for the refrigerant mass flux G varying from 300 to 600 kg/m^{2}s, imposed heat flux q from 0 to 45 kW/m^2, inlet liquid subcooling ΔT_{sub} from 3 to 6 °C, and system pressure P set at 776 kPa and 899 kPa (corresponding to T_{sat} = 10 °C and 15 °C) for the gap of the duct δ = 1.0 and 2.0 mm. The ranges of the parameters chosen above are in accordance with some air-conditioning applications. The measured boiling heat transfer data are expressed in terms of the boiling curves and boiling heat transfer coefficient. Moreover, selected flow photos and data deduced from the images of the boiling processes taken at a small region around the middle axial station z = 80 mm are presented to illustrate the bubble characteristics in the boiling flow.

Table 1
Summary of the results from uncertainty analysis.

Parameter	Uncertainty
Annular pipe geometry	
Length, width and thickness (%)	±1.0%
Area (%)	±2.0%
Parameter measurement	
Temperature, T (°C)	±0.2
Temperature difference, $^{\Delta}$T (°C)	±0.3
System pressure, P (kPa)	±2
Mass flux of refrigerant, G (%)	±2
Subcooled flow boiling heat transfer	
Imposed heat flux, q (%)	±4.5
Heat transfer coefficient, h_r (%)	±14

4.1. Subcooled flow boiling curves

The effects of the experimental parameters including the R-407C refrigerant mass flux, inlet subcooling, saturated temperature and the gap size of the duct on the subcooled boiling curves measured at the middle axial location of the duct are illustrated in Fig. 3. The results in Fig. 3 indicate that for a given boiling curve, at low imposed heat flux the temperature of the heated wall is below T_{sat} of R-407C and heat transfer in the duct is completely due to the single-phase forced convection. As the imposed heat flux is raised gradually, the heated wall temperature increases slowly to exceed T_{sat} at a certain q and we have a positive wall superheat ΔT_{sat} (T_w–T_{sat}). When ΔT_{sat} reaches a certain critical level, a small increase in q causes boiling to suddenly appear on the heated wall and the heated wall temperature drops immediately to a noticeable degree. Thus, there is a significant temperature overshoot during the onset of nucleate boiling (ONB) in the subcooled flow boiling. Note that the temperature overshoot can be as high as 5.8 °C for G = 600 kg/m^{2}s, δ = 1.0 mm, T_{sat} = 15 °C and ΔT_{sub} = 3 °C (Fig. 3(a)). Note that the influence of the refrigerant mass flux on the magnitude of the temperature overshoot during ONB is slight. Besides, a slightly higher wall superheat is needed to initiate the nucleate boiling for a higher G due to the thinner thermal boundary layer on the heated surface. Beyond the ONB, a small rise in ΔT_{sat} causes a large increase in the wall heat transfer rate and the slopes of the boiling curves are much steeper than those for the single-phase convection. Checking further with the data in Fig. 3(a) reveals that beyond ONB, the refrigerant mass flux exhibits rather slight effects on the boiling curves. Nevertheless, in the single-phase region the heated wall temperature is somewhat affected by the refrigerant mass flux. The higher G causes the higher liquid velocity in the channel resulting in a shorter time for the refrigerant to be heated. Thus, the imposed heat flux needed to initiate ONB is larger at a higher mass flux.

Next, the effects of the inlet liquid subcooling on the subcooled boiling curves are shown in Fig. 3(b). Note that higher wall superheat and higher imposed heat flux are needed to initiate the boiling on the heated surface for a higher ΔT_{sub}. It is also noted that the boiling curves are not affected to a noticeable degree by the inlet liquid subcooling in the two-phase region. However, in the single-phase region a higher liquid subcooling results in a higher heat transfer from the heated wall to the refrigerant flow.

Then, the effects of the refrigerant saturated temperature on the subcooled boiling curves are exemplified in Fig. 3(c). It is noted that higher ΔT_{sat} and q are needed to achieve ONB for a lower saturated temperature. This is attributed to the fact that at a lower $T_{sat,}$ the surface tension of R-407C is higher. At the higher surface-tension, the liquid refrigerant is more difficult to completely flood the cavities, which in turn retards the bubbles to nucleate from the cavities on the heated surface. Otherwise, the effect of T_{sat} on the boiling curves is rather slight.

Finally, the effects of the duct gap on the subcooled boiling curves are shown in Fig. 3(d). It is noted that somewhat lower wall superheat and imposed heat flux are needed to initiate the boiling on the heated surface for a smaller δ. This primarily results from the fact that for given G, q, T_{sat} and $\Delta T_{sub,}$ the mass flow rate through the duct is lower for a smallerδ. Thus, the axial temperature rise of the refrigerant flow is larger for a smaller δ, which results in a required lower ΔT_{sat} and q at ONB. It is also noted that the boiling curves are shifted significantly to the left in the nucleate boiling region as the gap size is decreased, indicating that the boiling heat transfer in the duct with a smaller gap is much better.

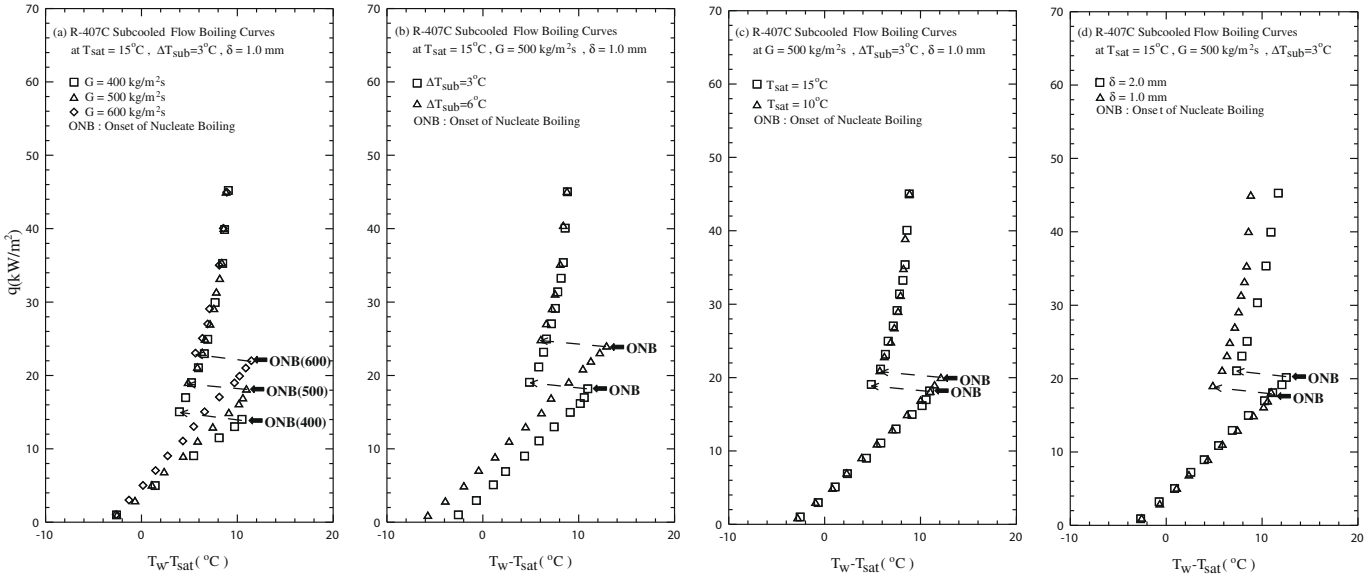

Fig. 3. Subcooled flow boiling curves of R-407C: (a) for various refrigerant mass fluxes at T_{sat} = 15 °C, ΔT_{sub} = 3 °C and δ = 1 mm, (b) for various inlet subcoolings at T_{sat} = 15 °C, G = 500 kg/m^{2}s and δ = 1 mm, (c) for various saturated temperatures at G = 500 kg/m^{2}s, ΔT_{sub} = 3 °C and δ = 1 mm, and (d) for various gap sizes at T_{sat} = 15 °C, G = 500 kg/m^{2}s and ΔT_{sub} = 3 °C.

4.2. Subcooled flow boiling heat transfer coefficients

The R-407C subcooled flow boiling heat transfer coefficients measured at the middle axial location (z = 80 mm) in the narrow annular duct affected by the four experimental parameters are shown in Fig. 4. The results in Fig. 4 indicate that the increase of h_r with the imposed heat flux is relatively significant for all cases. We note from Fig. 4(a) that the refrigerant mass flux exhibits only a rather slight effect on the boiling heat transfer coefficient. Besides, the boiling heat transfer is much better with a smaller inlet liquid subcooling (Fig. 4(b)). For instance, at q = 40 kw/m^2, T_{sat} = 15 °C, G = 500 kg/m^{2}s and δ = 1.0 mm, h_r for ΔT_{sub} = 3 °C is about 14% higher than that for ΔT_{sub} = 6°C (Fig. 4(b)). Then, the refrigerant saturated temperature shows relatively slight effects on the boiling heat transfer coefficient (Fig. 4(c)). It is of interest to note from the data in Fig. 4(d) that reducing the duct size can effectively enhance the subcooled boiling heat transfer in the duct. For the specific case with q = 40 kw/m^2, T_{sat} = 15°C, G = 500 kg/m^{2}s and ΔT_{sub} = 3°C, h_r for δ = 1.0 mm is about 40% higher than that for δ = 2.0 mm (Fig. 4(d)). This is considered to mainly result from the fact that in the narrower duct the radial gradient of the liquid axial velocity is larger, which in turn exerts higher shear force on the bubbles nucleated from the wall and causes them to depart from the heating surface at a higher rate.

It is noted that for each case the data in Fig. 3 for the boiling curves allow us to read the heated surface temperature and then the data in Fig. 4 for the boiling heat transfer coefficient can be used to find the refrigerant temperature at the middle axial location. Finally, the refrigerant temperature at the duct outlet can be evaluated from Eq. (2).

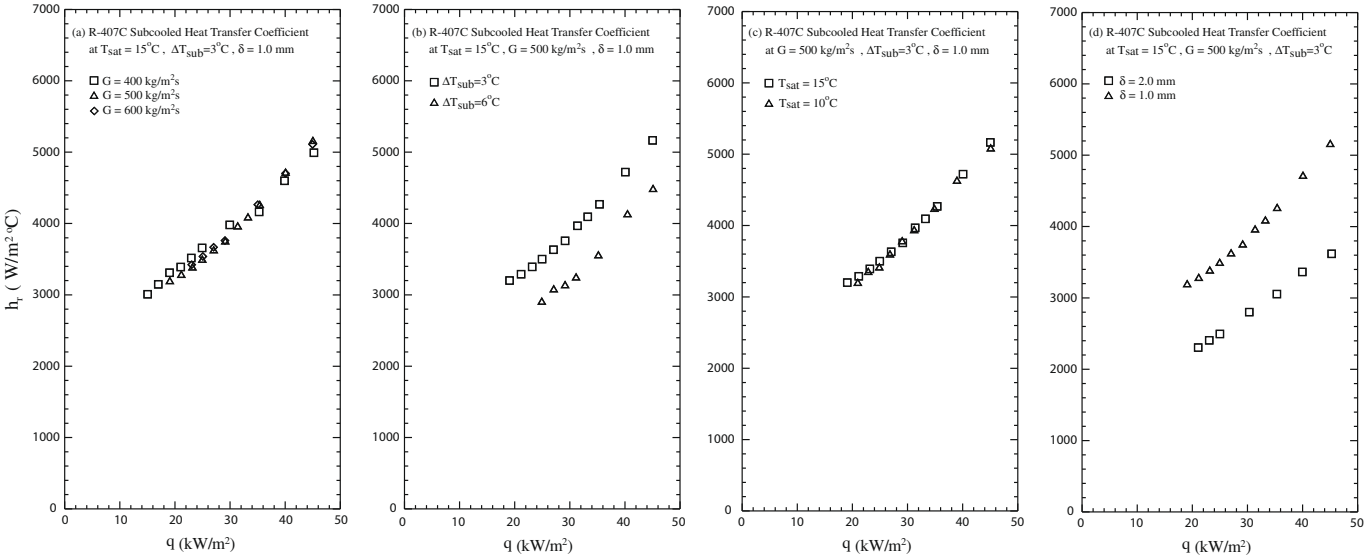

Fig. 4. Subcooled flow boiling heat transfer coefficient of R-407C: (a) for various refrigerant mass fluxes at T_{sat} = 15 °C, ΔT_{sub} = 3 °C and δ = 1 mm, (b) for various inlet subcoolings at T_{sat} = 15 °C, G = 500 kg/m^{2}s and δ = 1 mm, (c) for various saturated temperatures at G = 500 kg/m^{2}s, ΔT_{sub} = 3 °C and δ = 1 mm, and (d) for various gap sizes at T_{sat} = 15 °C, G = 500 kg/m^{2}s and ΔT_{sub} = 3 °C.

4.3. Bubble characteristics in subcooled flow boiling

To reveal the bubble characteristics, the photos of the R-407C boiling flow for the cases at selected experimental conditions taken from a small region around the middle axial location are shown in Fig. 5. First, the bubbles at the low q of 25 kW/m^2 for the case at T_{sat} = 15 °C, G = 500 kg/m^{2}s, δ = 1.0 mm and ΔT_{sub} = 3 °C can be seen from Fig. 5(a). Checking with the video tapes recording the bubble motion discloses that the bubbles form and grow at the active nucleation sites while they experience a short period of stationary growth to a certain size and then detach from the heating surface and accelerate into the subcooled liquid refrigerant. As the imposed heat flux is increased slightly to q = 35 kW/m^2 (Fig. 5(b)), more bubbles are nucleated and they collide and coalesce occasionally. The coalesced bubbles rise faster than the tiny bubbles due to the larger buoyancy force associated with them. Coalescence of the bubbles occurs more frequently and irregularly as the imposed heat flux is raised to 45 kW/m^2 (Fig. 5(c)). In general, increasing the imposed heat flux directly provides more energy to the cavities and more cavities on the heating surface can be activated. Besides, the higher buoyancy from the higher wall superheat causes the bubble departure frequency to increase substantially with the imposed heat flux. Moreover, the bubble departure diameter increases slightly with the imposed heat flux due to the higher wall superheat.

Next, Figs. 5(d)–(f) show the bubble characteristics around the middle axial location affected by the refrigerant mass flux by presenting the photos for the higher G of 600 kg/m^{2}s but at the same q, T_{sat}, δ and ΔT_{sub} as that for Figs. 5(a)–(c). The higher speed of the refrigerant flow for a higher G can sweep the bubbles more quickly away from the cavities resulting in a higher bubble departure frequency and the smaller bubble departure diameter. Besides, at a higher G the liquid temperature is lower for a given imposed heat flux at a given ΔT_{sub}. Thus, less bubble nucleation is activated on the heated wall and the bubble population falls.

Then, the effects of the inlet liquid subcooling on the bubble characteristics are illustrated by comparing the photos shown in Figs. 5(g)–(i) with Figs. 5(a)–(c) respectively for ΔT_{sub} = 6 °C and 3 °C at q = 25∼45 kW/m^2, G = 500 kg/m^{2}s, δ = 1.0 mm and T_{sat} = 15 °C. In general, the bubbles are larger at a lower liquid subcooling due to the weaker vapor condensation and more bubble coalescence at a lower ΔT_{sub}. In addition, an increase in the inlet subcooling results in the reduction of the bubble departure frequency and active nucleation sites. This is due to the fact that at a higher ΔT_{sub}, the liquid R-407C temperature at the subcooled liquid–vapor interface is relatively low compared to the hot heated surface. Thus the wall superheat is not high enough to sustain the continuing growth of the bubbles for an increase in ΔT_{sub}.

Additionally, the effects of the refrigerant saturation temperature on the bubble characteristics are exemplified by comparing the photos shown in Figs. 5(j)–(l) with Figs. 5(a)–(c) respectively for T_{sat} = 10°C and 15°C at q = 25∼45 kW/m^2, G = 500 kg/m^{2}s, δ = 1.0 mm and ΔT_{sub} = 3°C. In general, bubbles are larger due to the higher surface tension at a lower saturation temperature with more bubble coalescence. Besides, the active nucleation sites increase with increasing T_{sat} due to lower surface tension and enthalpy of vaporization.

Finally, the bubble characteristics affected by the duct size are shown by comparing the results in Fig. 5(m)–(o) with Fig. 5(a)–(c). It is noted that the bubbles are slightly bigger in the smaller duct. Besides, the bubble departure frequency is higher. The larger bubbles collide and coalesce more frequently in the narrower duct. It is due to the larger axial temperature rise of the refrigerant flow with a smaller duct gap, which in turn results in a higher liquid temperature at the interface between gas and liquid. Thus, more large bubbles are formed from the coalescence of the small bubbles in the smaller ducts. As the heat flux is raised to q = 45 kW/m^2 (Figs. 5(c) and (o)), the bubbles in the smaller duct coalesce even more frequently and the large bubbles somewhat deform due to the space limitation.

To be quantitative on the bubble characteristics, we video tape the motion of bubbles and estimate the mean bubble departure diameter, frequency and the active nucleation site density in the bubbly flow by carefully tracing the bubble motion from the images of the boiling flow. The outcomes from this estimation

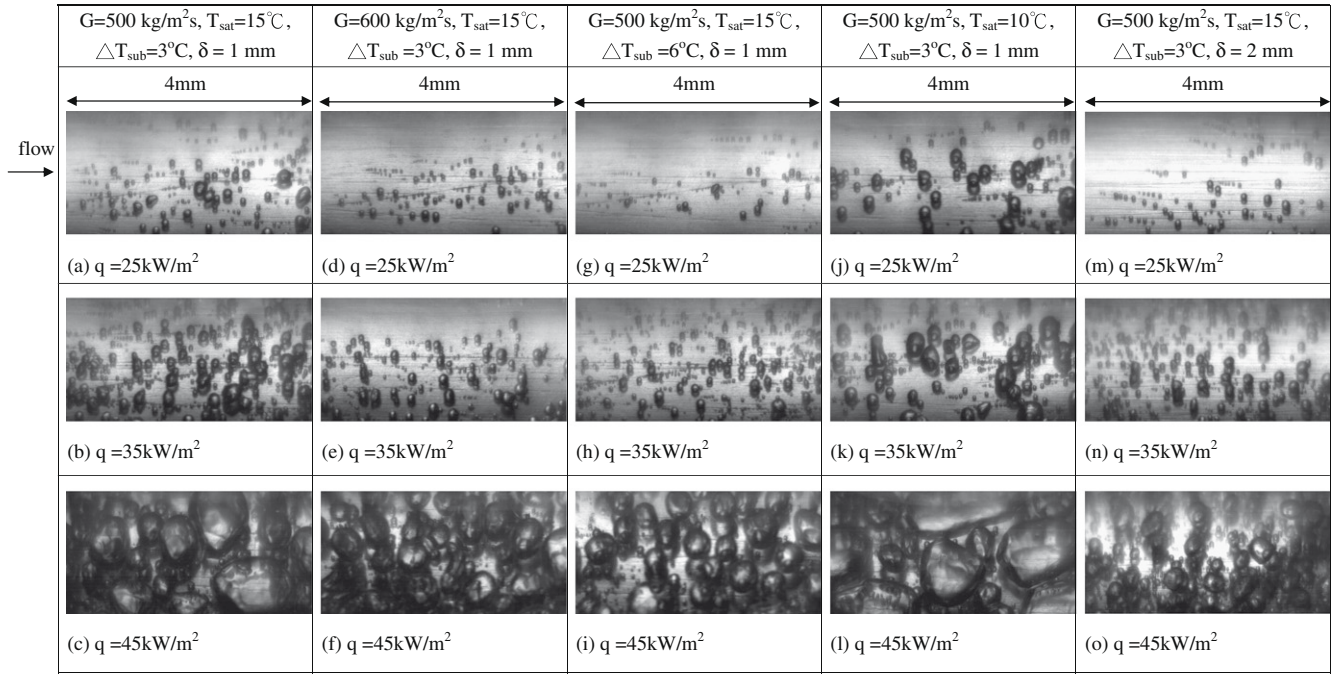

Fig. 5. Photos of bubbles in the subcooled flow boiling of R-407C in a small region around middle axial location for various imposed heat fluxes, mass fluxes, inlet liquid subcoolings, saturated temperatures and gap sizes.

are examined in the following. The effects of the four experimental parameters on the mean bubble departure diameter for the R-407C subcooled flow boiling at the middle axial location (z = 80 mm) of the annular duct are shown in Fig. 6. Note that the increase of the bubble departure size with the heat flux is very significant for all cases presented here. Besides, the effects of the refrigerant mass flux shown in Fig. 6(a) indicate that the average bubble departure diameter d_p is slightly larger for a smaller G. It is also noted that d_p is somewhat larger for a smaller liquid subcooling (Fig. 6(b)). Moreover, at a higher T_{sat} the average departing bubble is slightly smaller (Fig. 6(c)). Furthermore, the average departing bubbles are slightly larger in the narrower duct especially at high imposed heat flux (Fig. 6(d)). It is worth mentioning that even the size of the largest departing bubble is below 0.15 mm which is much smaller than the diameter of the outer glass pipe in the test section (D_p = 20.0 mm). Thus the observation of the bubble size through the curved surface of the glass pipe is not expected to produce significant error.

How the bubble departure frequency is affected by the four parameters for the subcooled R-407C flow boiling at the middle axial location in the annular duct are shown in Fig. 7. Note that the increase of the bubble departure frequency with the imposed heat flux is rather significant for all cases presented here. Besides, the bubble departure frequency is higher with higher refrigerant mass flux and saturated temperature. However, the bubble departing rate reduces at increasing duct size and liquid subcooling.

The associated density of the active nucleation sites affected by the four parameters is shown in Fig. 8. Again, for all cases the increase of the average active nucleation site density with the imposed heat flux is rather pronounced. It is also noted that the active nucleation site density is higher with lower refrigerant mass flux, lower liquid subcooling and higher refrigerant saturated temperature especially at high imposed heat flux. Besides, the influence of the duct size on the average active nucleation site density is insignificant.

4.4. Comparison with data for subcooled R-134a flow boiling

We move further to compare the present data for the R-407C subcooled flow boiling with that for R-134a subcooled flow boiling from Lie [27] measured in the same narrow annular duct in Fig. 9. The data from the boiling curves in Fig. 9(a) indicate that a slightly higher wall superheat is needed to initiate boiling for R-134a. This can be attributed to the lower surface tension for R-407C. Besides, the slope of the boiling curve for R-407C is much steeper, suggesting the subcooled flow boiling heat transfer for R-407C is much better. Indeed, the data in Fig. 9(b) manifest that R-407C has a much higher boiling heat transfer coefficient except at the low heat flux near ONB.

4.5. Comparison with some existing correlations

Moreover, in Fig. 10 the present data for the R-407C subcooled flow boiling heat transfer coefficient are compared with some existing empirical correlations proposed in the open literature. Note that the correlations from Shah [19] and Kandlikar [24] substantially over-predict our data. Similarly, the correlations from Bao et al. [4], Tran et al. [5], Liu and Winterton [20] also over-predict our data to some degree. However, our data are well correlated by the correlation of Fujita et al. [23]. The correlation of Fujita el al. is

$$h_r = 0.884G^{0.143}q^{0.714} \tag{3}$$

4.6. Correlation equations

According to flow boiling mechanisms [17], heat transfer in the bubbly flow regime in the flow boiling can be roughly considered as a combination of single-phase liquid forced convection heat transfer q_c and pool boiling heat transfer q_b. Thus, the total heat flux input to the boiling flow q_t can be expressed as

$$q_t = q_b + q_c \tag{4}$$

Here q_b and q_c can be respectively calculated from the relations

$$q_b = \rho_g V_g f N_{ac} i_{fg} \tag{5}$$

and

$$q_c = Eh_l(T_w - T_r) \tag{6}$$

Note that in the above equation, an enhancement factor E is added to q_c to account for the agitating motion of the bubbles which can enhance the single-phase convection heat transfer. Empirically, E and h_1 can be correlated as

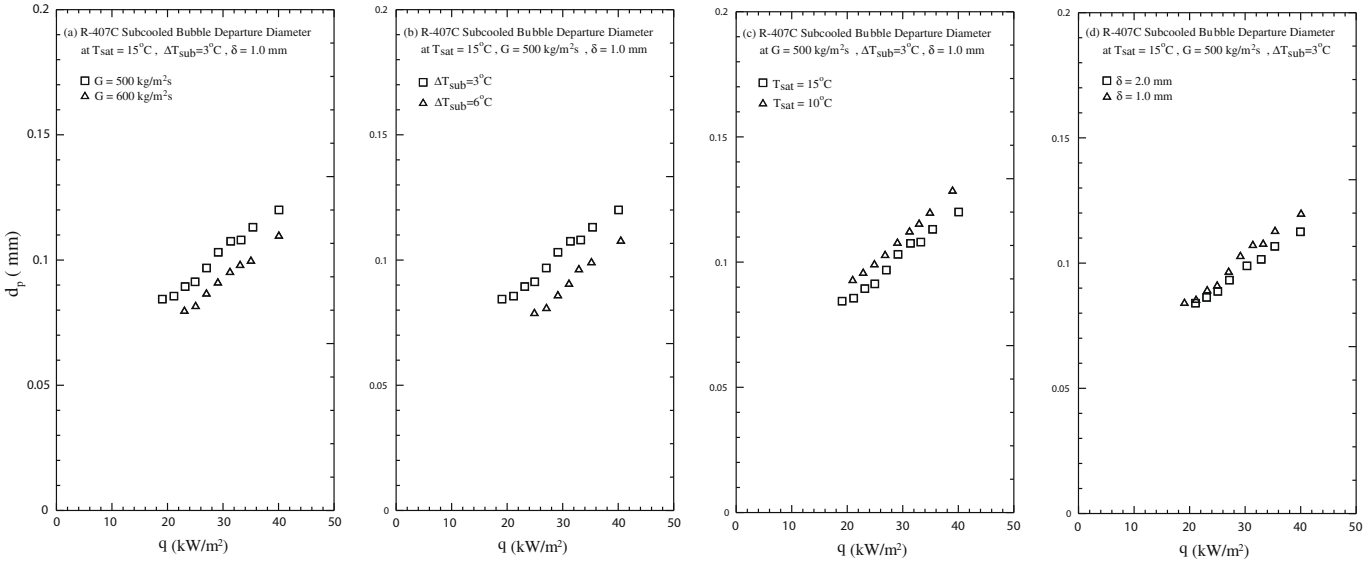

Fig. 6. Mean bubble departure diameter for subcooled flow boiling of R-407C: (a) for various refrigerant mass fluxes at T_{sat} = 15 °C, ΔT_{sub} = 3 °C and δ = 1 mm, (b) for various inlet subcoolings at T_{sat} = 15 °C G = 500 kg/m^{2}s and δ = 1 mm, (c) for various saturated temperatures at G = 500 kg/m^{2}s, ΔT_{sub} = 3 °C and δ = 1 mm, and (d) for various gap sizes at T_{sat} = 15°C, G = 500 kg/m^{2}s, ΔT_{sub} = 3 °C.

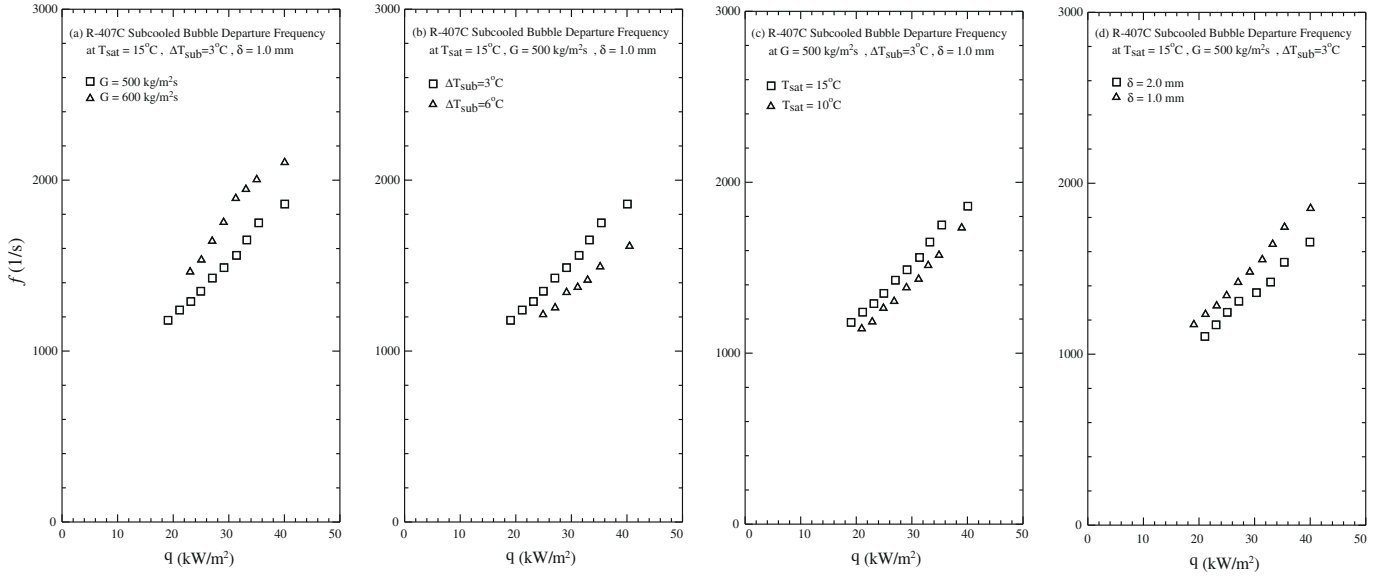

Fig. 7. Mean bubble departure frequency for subcooled flow boiling of R-407C: (a) for various refrigerant mass fluxes at T_{sat} = 15 °C, ΔT_{sub} = 3 °C and δ = 1 mm, (b) for various inlet subcoolings at T_{sat} = 15 °C G = 500 kg/m^{2}s and δ = 1 mm, (c) for various saturated temperatures at G = 500 kg/m^{2}s, ΔT_{sub} = 3 °C and δ = 1 mm, and (d) for various gap sizes at T_{sat} = 15 °C, G = 500 kg/m^{2}s, ΔT_{sub} = 3 °C.

$$E = \max\left(1, N_{conf}^{0.2} Fr_1^{0.01}(1+200Bo)^5\right) \tag{7}$$

and

$$h_l = Nu_l k_l / D_h \tag{8}$$

Note that Nu_1 is estimated from the Gnielinski correlation [31],

$$Nu_l = \frac{(f_f/8)(Re_1 - 1000)Pr_1}{1 + 12.7\sqrt{f_f/8}(Pr^{2/3} - 1)} \qquad for\ Re_1 \geqslant 2300 \tag{9}$$

Here the friction factor f_f is evaluated from the relation

$$f_f = (1.82 \times \log_{10} Re_1 - 1.64)^{-2} \tag{10}$$

In Eq. (5) ρ_g is the vapor density, V_g is the mean vapor volume of the departing bubble which is equal to $\frac{4\pi}{3}(\frac{d_p}{2})^3$, f is the mean bubble departure frequency, N_{ac} is the mean active nucleation site density, and i_{fg} is the enthalpy of vaporization. Since the experimental Re_l ranges from 5400 to 11,500, we use the Gnielinski correlation for Re_l > 2300 to evaluate the single-phase forced convection heat transfer. It is difficult to distinguish the individual bubbles at a higher imposed heat flux. Hence the above correlations do not apply to the data for q > 40 kW/m^2.

To enable the usage of the above correlation for computing the flow boiling heat transfer in the bubbly flow regime, the mean departing bubble size and frequency and the mean active nucleation site density on the heating surface need to be correlated in

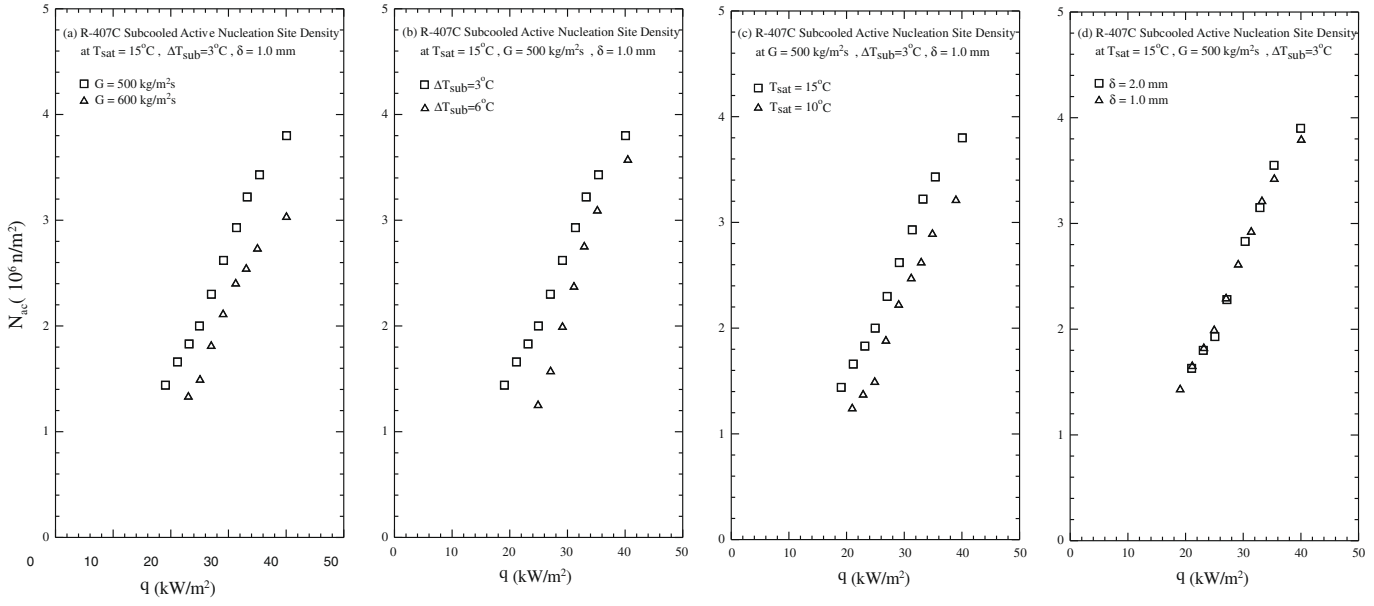

Fig. 8. Mean active nucleation site density for subcooled flow boiling of R-407C: (a) for various refrigerant mass fluxes at T_{sat} = 15 °C, ΔT_{sub} = 3 °C and δ = 1 mm, (b) for various inlet subcoolings at T_{sat} = 15 °C G = 500 kg/m^{2}s and δ = 1 mm, (c) for various saturated temperatures at G = 500 kg/m^{2}s, ΔT_{sub} = 3 °C and δ = 1 mm, and (d) for various gap sizes at T_{sat} = 15 °C, G = 500 kg/m^{2}s, ΔT_{sub} = 3 °C.

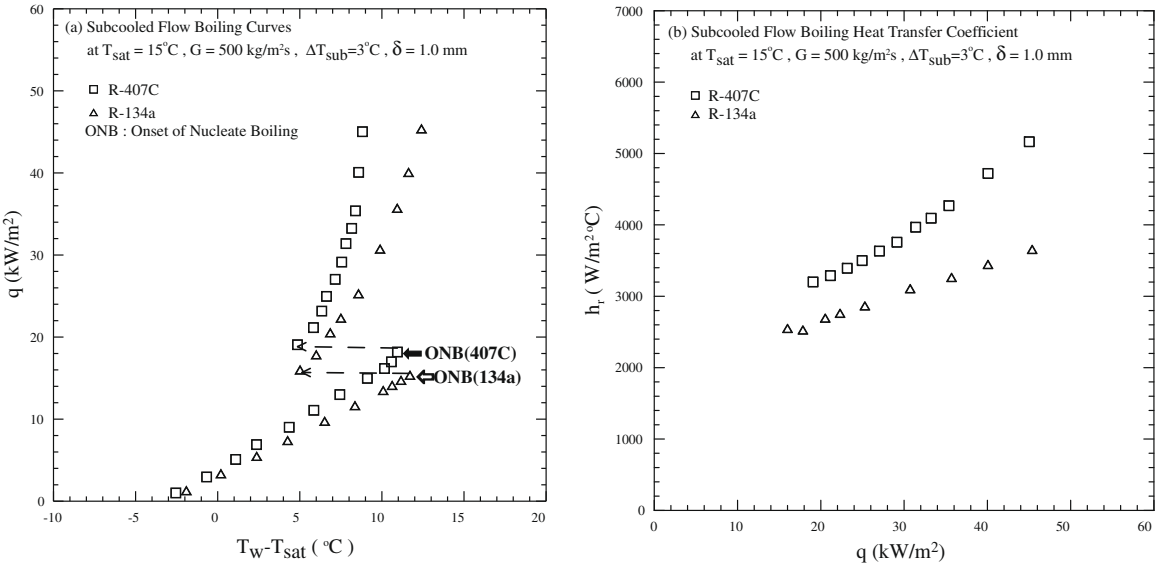

Fig. 9. Comparison of R-407C and R-134a subcooled flow boiling.

advance. The average bubble departure diameter in the R-407C subcooled flow boiling in the narrow annular duct estimated from the present flow visualization can be correlated as

$$D_p = \frac{d_p}{\sqrt{\sigma/(g\Delta\rho)}} = \frac{160N_{conf}(\rho_1/\rho_g)^{0.6}}{Re_l^{0.5}\left[Ja + \frac{150(\rho_1/\rho_g)^{0.9}}{BoRe_l^{1.4}}\right]} \tag{11}$$

Here Ja is the Jakob number defined as

$$Ja = \frac{\rho_1 \cdot C_p \cdot \Delta T_{sub}}{\rho_g \cdot i_{fg}} \tag{12}$$

Fig. 11(a) shows that almost all the present experimental data for d_p fall within ±25% of the above correlation and the mean absolute error is 13.3%. Besides, an empirical equation is proposed for the product of the mean bubble departure diameter and frequency as

$$F_d = \frac{f \cdot d_p}{\mu_1/(\rho_1 D_h)} = 1600 \cdot Re_1^{0.887} \cdot Ja^{-0.05} \cdot Bo^{0.887} \cdot N_{conf}^{0.3} \tag{13}$$

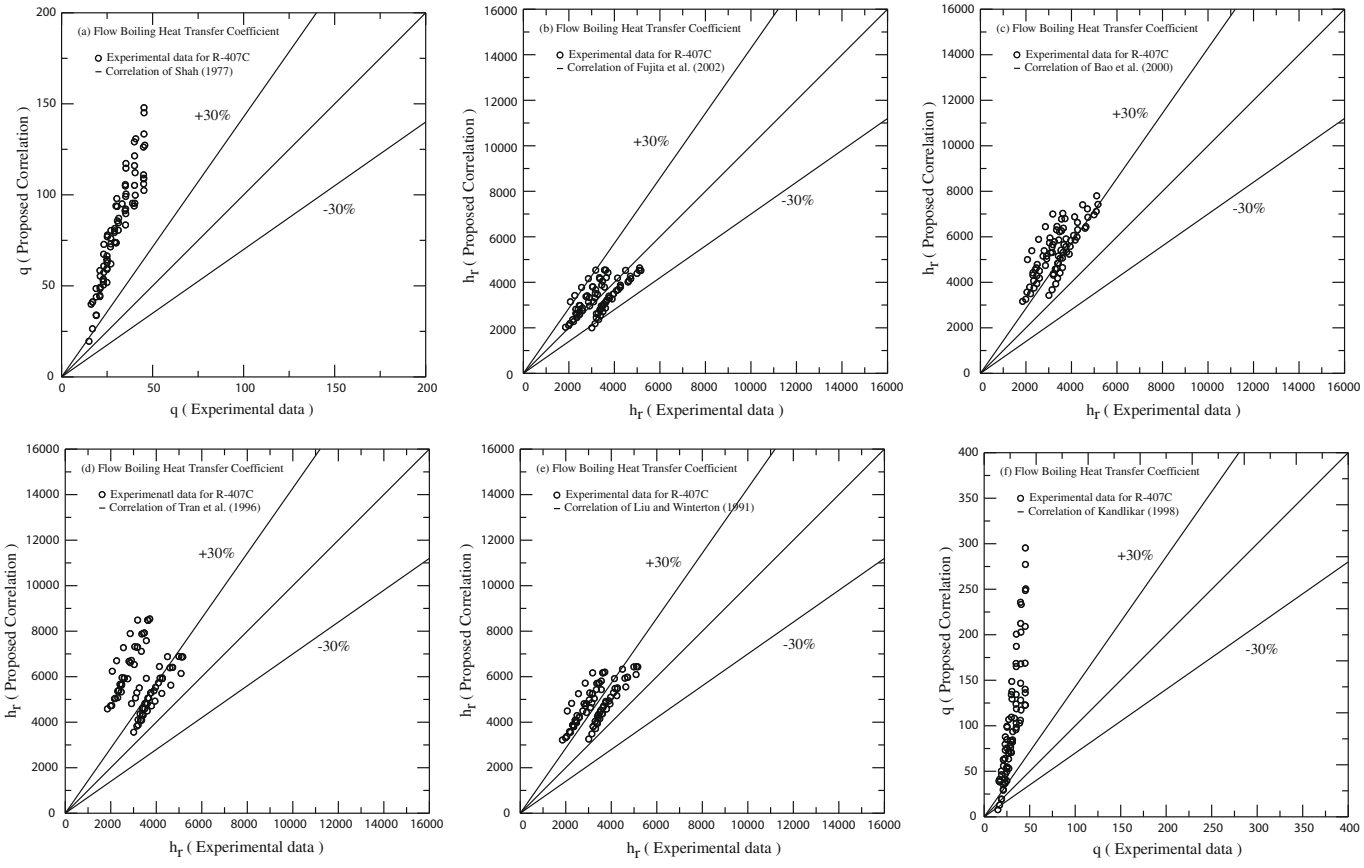

Fig. 10. Comparison of the present data for heat transfer coefficient in the subcooled flow boiling of R-407C with existing correlations.

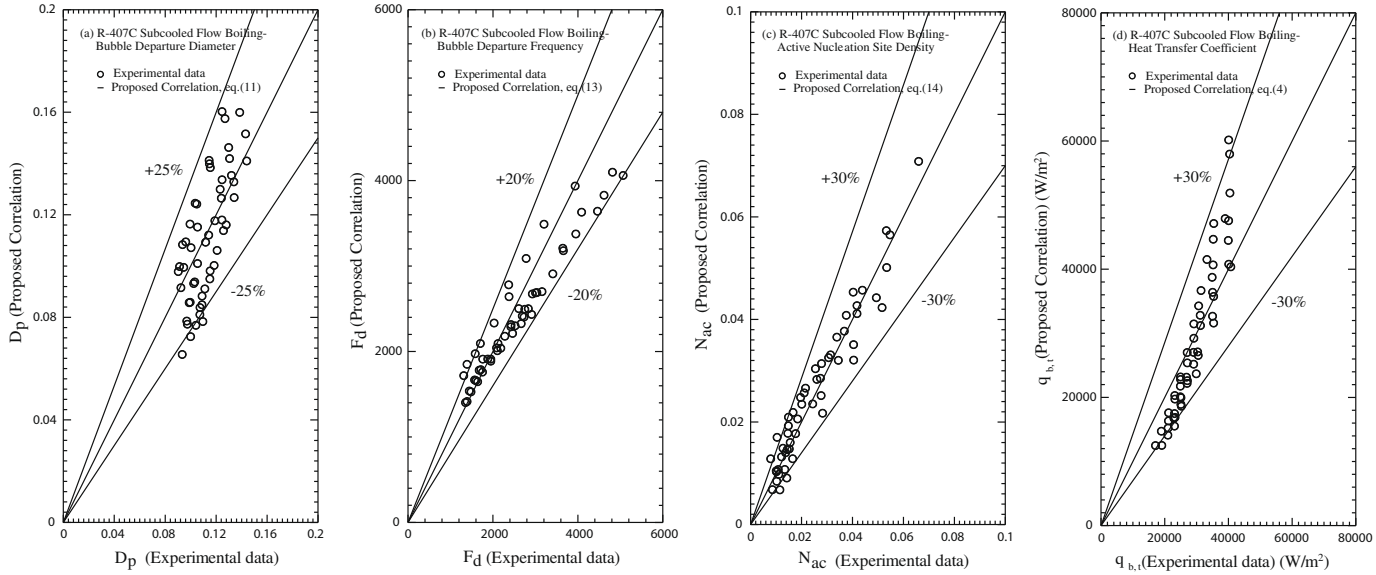

Fig. 11. Comparison of the measured data for mean bubble departure diameter (a), mean bubble departure frequency (b), mean active nucleation site density (c), and heat transfer coefficient (d) in the subcooled flow boiling of R-407C with the proposed correlations.

Note that almost all the experimental data for $f \cdot d_p$ collected in this study can be correlated within ±20% by Eq. (13) and the mean absolute error is 10% (Fig. 11(b)). Finally, we propose an empirical correlation for the average active nucleation site density in the R-407C subcooled flow boiling as

$$N_{AC} = n_{ac} d_p^2 = -0.035 + 1700 Bo \cdot Re_1^{-0.25} \cdot Ja^{-0.25} \cdot N_{conf}^{-0.05} \qquad (14)$$

Fig. 11(c) shows that nearly all the present experimental data fall within ±30% of the above correlation and the mean absolute error is 14.8%.

When the correlations for d_p, f, and n_{ac} given in Eqs. (11)–(14) are combined with Eqs. (4)–(10) for q_t, more than 90% of the heat transfer data for the bubbly flow regime measured in the present study fall within ±30% of the correlation proposed here with a mean deviation of 17.3% (Fig. 11(d)).

5. Concluding remarks

The experimental heat transfer data for the subcooled flow boiling of R-407C in the narrow annular duct have been presented here along with the bubble behavior in the boiling flow. Effects of the imposed heat flux, refrigerant mass flux, inlet subcooling, saturated temperature, and duct size on the R-407C subcooled flow boiling heat transfer and associated bubble characteristics have been investigated. Moreover, comparison of the present data with some existing correlations is conducted. The major outcomes obtained here can be summarized in the following.

(1) The temperature overshoot at ONB is significant for the subcooled flow boiling of R-407C in the narrow annular duct.
(2) The subcooled boiling heat transfer coefficient increases with a decrease in the duct size, but decreases with an increase the inlet subcooling. Besides, raising the imposed heat flux can cause a significant increase in the boiling heat transfer coefficients. However, the effects of the refrigerant mass flux and saturated temperature on the boiling heat transfer coefficient are small but cannot be entirely neglected in the narrow duct examined here.
(3) Visualization of the bubble motion in the boiling flow reveals that the bubbles are suppressed by raising the refrigerant mass flux and inlet subcooling. The mean bubble departure diameter, mean bubble departure frequency and active nucleation site density reduce at increasing inlet subcooling. Moreover, raising the imposed heat flux produces positive effects on the bubble population, coalescence and departure frequency.
(4) The boiling heat transfer coefficient, mean bubble departure diameter, bubble departure frequency and active nucleation site density in the R-407C subcooled flow boiling are correlated in terms of the relevant dimensionless groups.

Acknowledgment

The financial support of this study by the engineering division of National Science Council of Taiwan, R.O.C. through the contract NSC 96-2221-E-009-133-MY3 is greatly appreciated.

References

[1] S.M. Ghiaasiaan, Two-Phase Flow Boiling, and Condensation in Conventional and Miniature Systems, Cambridge, 2008.
[2] S.G. Kandlikar, W.J. Grande, Evolution of microchannel flow passages – thermohydraulic performance and fabrication technology, Heat Transfer Eng. 24 (1) (2003) 3–17.
[3] P.A. Kew, K. Cornwell, Correlations for the prediction of boiling heat transfer in small-diameter channels, Appl. Thermal Eng. 17 (1997) 705–715.
[4] Z.Y. Bao, D.F. Fletcher, B.S. Haynes, Flow boiling heat transfer of Freon R11 and HCFC123 in narrow passages, Int. J. Heat Mass Transfer 43 (18) (2000) 3347–3358.
[5] T.N. Tran, M.W. Wambsganss, D.M. France, Small circular- and rectangular-channel boiling with two refrigerants, Int. J. Multiphase Flow 22 (1996) 485–498.
[6] B. Agostini, A. Bontemps, Vertical flow boiling of refrigerant R134a in small channels, Int. J. Heat Fluid Flow 26 (2005) 296–306.
[7] S.G. Kandlikar, M.E. Steinke, Flow boiling heat transfer coefficient in minichannels – correlation and trends, Proc. Twelfth Int. Heat Transfer Conf. vol. 1.3 (2002) 785–790.
[8] S. Lin, P.A. Kew, K. Cornwell, Two-phase heat transfer to a refrigerant in a 1 mm diameter tube, Int. J. Refrig. 24 (1) (2001) 51–56.
[9] B. Watel, Review of saturated flow boiling in small passages of compact heat exchangers, Int. J. Thermal Sci. 42 (2003) 107–140.
[10] S.H. Chang, I.C. Bang, W.P. Baek, A photographic study on the near-wall bubble behavior in subcooled flow boiling, Int. J. Thermal Sci. 41 (2002) 609–618.

[11] R. Situ, Y. Mi, M. Ishii, M. Mori, Photographic study of bubble behaviors in forced convection subcooled boiling, Int. J. Heat Mass Transfer 47 (2004) 3659–3667.
[12] C.P. Yin, Y.Y. Yan, T.F. Lin, B.C. Yang, Subcooled flow boiling heat transfer of R-134a and bubble characteristics in a horizontal annular duct, Int. J. Heat Mass Transfer 43 (2000) 1885–1896.
[13] R. Maurus, V. Ilchenko, T. Sattelmayer, Automated high-speed video analysis of the bubble dynamics in subcooled flow boiling, Int. J. Heat Fluid Flow 25 (2004) 149–158.
[14] T. Okawa, T. Ishida, I. Kataoka, M. Mori, An experimental study on bubble rise path after the departure from a nucleation site in vertical upflow boiling, Exp. Thermal Fluid Sci. 29 (2005) 287–294.
[15] G.E. Thorncroft, J.F. Klausner, R. Mei, An experimental investigation of bubble growth and detachment in vertical upflow and downflow boiling, Int. J. Heat Mass Transfer 41 (23) (1998) 3857–3871.
[16] O. Zeitoun, M. Shoukri, Bubble behavior and mean diameter in subcooled flow boiling, ASME J. Heat Transfer 118 (1996) 110–116.
[17] J.C. Chen, A correlation for boiling heat transfer to saturated fluids in convective flow, Ind. Eng. Chem. Process Design Dev. 5 (1966) 322–329.
[18] K.E. Gungor, R.H.S. Winterton, A general correlation for flow boiling in tubes and annuli, Int. J. Heat Mass Transfer 29 (1986) 351–358.
[19] M.M. Shah, A general correlation for heat transfer during subcooled boiling in pipes and annuli, ASHRAE Trans. 83 (1977) 205–215.
[20] Z. Liu, R.H.S. Winterton, A general correlation for saturated and subcooled flow boiling in tubes and annuli, based on a nucleate pool boiling equation, Int. J. Heat Mass Transfer 34 (1991) 2759–2766.
[21] W. Zhang, T. Hibiki, K. Mishima, Correlation for flow boiling heat transfer in mini-channels, Int. J. Heat Mass Transfer 47 (2004) 5749–5763.
[22] G.M. Lazarek, S.H. Black, Evaporative heat transfer, pressure drop and critical heat flux in a small vertical tube with R-113, Int. J. Heat Mass Transfer 25 (7) (1982) 945–960.
[23] Y. Fujita, Y. Yang, N. Fujita, Flow boiling heat transfer and pressure drop in uniformly heated small tubes, Proc. Twelfth Int. Heat Transfer Conf. 3 (2002) 743–748.
[24] S.G. Kandlikar, Heat transfer and flow characteristics in partial boiling, fully developed boiling, and significant void flow regions of subcooled flow boiling, ASME J. Heat Transfer 120 (1998) 395–401.
[25] S.G. Kandlikar, P. Balasubramanian, An extension of the flow boiling correlation to transition, laminar, and deep laminar flows in minichannles and microchannels, Heat Transfer Eng. 25 (2004) 86–93.
[26] F.C. Hsieh, K.W. Li, Y.M. Lie, C.A. Chen, T.F. Lin, Saturated flow boiling heat transfer of R-407C and associated bubble characteristics in a narrow annular duct, Int. J. Heat Mass Transfer 51 (2008) 3763–3775.
[27] Y.M. Lie, Heat transfer and bubble characteristics associated with flow boiling of refrigerant R-134a in a horizontal narrow annular duct, Ph.D. thesis, National Chiao Tung University, Taiwan, 2006.
[28] Y. M Lie, T.F. Lin, Subcooled flow boiling heat transfer and associated bubble characteristics of R-134a in a narrow annular duct, Int. J. Heat Mass Transfer 49 (13–14) (2006) 2077–2089.
[29] S.W. Churchill, H.H.S. Chu, Correlating equations for laminar and turbulent free convection from a horizontal cylinder, Int. J. Heat Mass Transfer 18 (1975) 1049–1053.
[30] S.J. Kline, F.A. McClintock, Describing uncertainties in single-sample experiments, ASME Mech. Eng. 75 (1) (1953).
[31] V. Gnielinski, New equations for heat and mass transfer in turbulent pipe and channel flow, Int. Chem. Eng. 16 (2) (1976) 359–368.